Magnetoelectric interactions in bismuth sodium-potassium titanate-nickel cobalt ferrite lead-free composite ceramics

J. Camargo, A. Prado Espinosa, F. Zabotto, L. Ramajo, M. Castro

PII: S0925-8388(20)30492-8

DOI: https://doi.org/10.1016/j.jallcom.2020.154129

Reference: JALCOM 154129

To appear in: *Journal of Alloys and Compounds*

Received Date: 25 November 2019

Revised Date: 23 January 2020

Accepted Date: 31 January 2020

Please cite this article as: J. Camargo, A. Prado Espinosa, F. Zabotto, L. Ramajo, M. Castro, Magnetoelectric interactions in bismuth sodium-potassium titanate-nickel cobalt ferrite lead-free composite ceramics, *Journal of Alloys and Compounds* (2020), doi: https://doi.org/10.1016/j.jallcom.2020.154129.

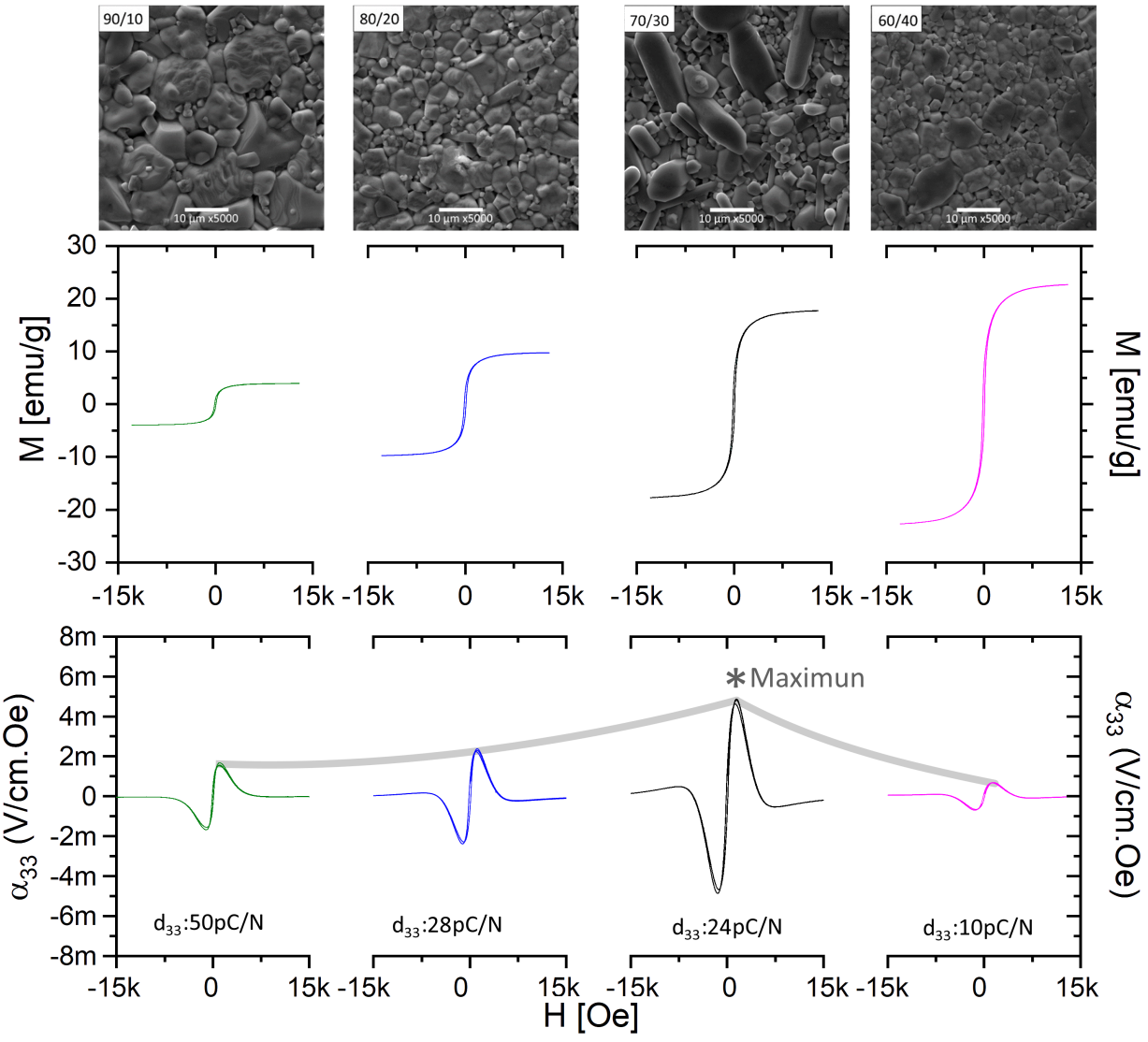
90/10
80/20
70/30
60/40
10 µm x5000
M [emu/g]
30
20
10
0
-10
-20
-30
-15k
0
15k
8m
6m
4m
2m
-2m
-4m
-6m
-8m
α33 (V/cm.Oe)
∗Maximun
d33:50pC/N
d33:28pC/N
d33:24pC/N
d33:10pC/N
H [Oe]

Magnetoelectric interactions in bismuth sodium-potassium titanate-nickel cobalt ferrite lead-free composite ceramics

J. Camargo[a], A. Prado Espinosa[a], F. Zabotto[b], L. Ramajo[a], M. Castro[a]

[a]Institute of Research in Materials Science and Technology (INTEMA), Av. Colón 10850 (7600), Mar del Plata, Argentina

[b]Physics Department, Federal University of São Carlos - UFSCar, CEP 13565-905, São Carlos, SP, Brazil

jcamargo@fi.mdp.edu.ar mcastro@fi.mdp.edu.ar

Abstract

Bismuth sodium-potassium titanate (BNKT) and nickel-cobalt ferrite (NCF) ceramic composite materials (*x*BNKT-(100-*x*)NCF), with different ferrite proportions, were studied. Piezoelectric and ferrite powders were separately synthesized by the solid-state method. Structural analyses were carried out by X-ray diffraction and Raman spectra studies of the composites whereas microstructural studies were performed by Scanning Electron Microscopy and the element distribution was studied by Energy Dispersive X-Ray Spectroscopy. Dielectric permittivity and loss values were sensitive to temperature and composition variations. Magnetic and magnetoelectric properties of the *x*BNKT-(100-*x*)NCF composites have been investigated. Ions diffusion and chemical reaction between BNKT and ferrite phases cause microstructural and structural variations that are responsible for moving away from the saturation magnetization from those calculated. Moreover, microstructural evolution controls the magnetoelectric properties of these lead-free composites.

Keywords: Magnetoelectricity, composites, Piezoelectricity, ferrite, Magnetic properties

Introduction

Magnetoelectric materials (ME) are one of the most important kinds of multiferroics that exhibit both magnetic and ferroelectric ordering. These materials are magnetized when subjected to an external electric field and electrically polarized when exposed to an external magnetic field [1]. ME materials have attracted enormous interest due to their potential applications in new multifunctional devices such as transducers, tunable filters, multi-state memories and field sensors, among others [2–4]. In recent years, a large number of studies have reported that the magnetoelectric voltage coupling coefficient (α_{ME}) in compounds containing a piezoelectric and a magnetostrictive material is several orders of magnitude greater than that of single-phase multiferroics [5–9].

A great magnetoelectric response has been reported in a variety of compounds consisting of $PbZr_{0.52}Ti_{0.48}O_3$ (PZT) or $Pb(Mg_{1/3}Nb_{2/3})_{0.67}Ti_{0.33}O_3$ (PMN-PT) as the piezoelectric phase and $CoFe_2O_4$ (CFO) or $NiFe_2O_4$ (NFO) ferrites as the magnetostrictive phase employing different configurations [3]. However, due to the toxicity of lead, which brings serious environmental and health complications, lead-free alternatives for piezoelectric and magnetoelectric ceramics must be found [10–12]. Studies on lead-free multiferroic magnetoelectric composites must be encouraged [1,13,14].

Recently, lead-free ceramics like $BaTiO_3$ (BT), $Bi_{0.5}Na_{0.5}TiO_3$ (BNT), $Sr_{0.5}Ba_{0.5}Nb_2O_6$ (SBN), $K_{0.5}Na_{0.5}NbO_3$ (KNN), and $82BaTiO_3$-$10BaZrO_3$-$8CaTiO_3$ (BZT–BCT) have been proposed as a piezoelectric phase in magnetoelectric compounds [15–22]. Specifically, BNT is one of the most promising piezoelectric perovskites due to its high Curie temperature (T_c~320 °C) and large remaining polarization (P_r~38 $\mu C/cm^2$). However, its higher coercive field and lower piezoelectric coefficient than other piezoelectric materials difficult its application [23,24]. It was established that the introduction of solid solutions can significantly improve the piezoelectric response of BNT ceramics. Specifically, the $Bi_{0.5}Na_{0.5}TiO_3$ (BNT)-$Bi_{0.5}K_{0.5}TiO_3$ (BKT) solid solution presents an increase in the piezoelectric coefficient close to the morphotropic phase boundary (MPB) region, where maximum d_{33} values and a coercive electric field diminution

have been reported for the 80BNT-20BKT composition [25–28].

In this work, a simple method to prepare the $xBi_{0.5}(Na_{0.8}K_{0.2})_{0.5}TiO_3$-$(100-x)Ni_{0.5}Co_{0.5}Fe_2O_4$ (xBNKT-(100-x)NCF) (x = 95, 90, 80 ,70, 60, 50) composite is presented. Piezoelectric and magnetic powders were separately synthesized by the solid-state reaction method and then mixed in several proportions and sintered. The main objective of this work is to understand how the relative composition of both phases affects the structure, microstructure, dielectric, piezoelectric, magnetic and magnetoelectric properties of BNT-NCF composites.

Experimental procedure

Powders of both $Ni_{0.5}Co_{0.5}Fe_2O_4$ (NCF) and $Bi_{0.5}(Na_{0.8}K_{0.2})_{0.5}TiO_3$ (BNKT) phases were previously synthesized by the solid-state reaction method. The NCF phase was obtained through the stoichiometric mixture of the reagents Cobalt acetate ($Co(C_2H_3O_2)_2$, commercial reagent), Nickel acetate ($Ni(C_2H_3O_2)_2$, Aldrich 99%, USA) and Hematite (Fe_2O_3, Mallinckrodt 97%, USA), as shown in Eq 1:

$$Co(C_2H_3O_2)_2 \cdot 4H_2O + Ni(C_2H_3O_2)_2 \cdot 4H_2O + 2\,Fe_2O_3 + 8\,O_2 \rightarrow 2\,Ni_{0.5}Co_{0.5}Fe_2O_4 + 8\,CO_2 + 14\,H_2O \quad (1)$$

To obtain the BNKT phase, the used reagents were Bismuth oxide (Aldrich 99.8%; USA), Sodium carbonate (Aldrich 99.5%; USA), Potassium carbonate (Aldrich 99.5%; USA) and Titanium oxide (Aldrich 99.9%; USA) according to Eq. 2:

$$Bi_2O_3 + 0.8\,Na_2CO_3 + 0.2\,K_2CO_3 + 4\,TiO_2 \rightarrow 4\,Bi_{0.5}(Na_{0.8}K_{0.2})_{0.5}TiO_2 + CO_2 + 2O_2 \quad (2)$$

The reagents of both phases were separately mixed for 6 hours in an alcoholic medium in a planetary mill (Fritsch, Pulverisette 7, 1050rpm). According to previous results, milled reactants were calcined at 700°C for the obtention of the BNKT phase free of secondary phases [29]. The calcination temperature of obtaining the ferrite phase free of hematite and secondary phases was determined from X-Ray Diffraction analyses (DRX, PANalytical, X´pert Pro, CuK_α).

After obtaining the individual phases, synthetized powders were mixed, according to $x Bi_{0.5}(Na_{0.8}K_{0.2})_{0.5}TiO_3$-(100-x)$Ni_{0.5}Co_{0.5}Fe_2O_4$, x = 50, 60, 70, 80 , 90, 95, for 3 hours again in alcoholic medium in a planetary mill at 1050rpm.

Subsequently, mixed powders were uniaxially pressed into discs and sintered at 1100°C for 5 hours. The obtained ceramics were characterized by X-ray Diffraction (DRX, PANalytical, X´pert Pro, CuK_α), Raman spectroscopy (Renishaw in Via microscope through of the 514 nm Ar-ion laser line) and Scanning Electron Microscopy (SEM, JEOL 6460LV, USA) with Energy Dispersive X-Ray Spectroscopy (EDS EDAX Genesis XM4-Sys 60, Japan). The bulk density of sintered ceramics was determined by the Archimedes method with distilled water as the immersion medium.

The dielectric behavior was analyzed on the sintered disks with silver electrodes painted on the surface. Dielectric properties were determined using an impedance analyzer (LCR meter HP4284A) in the temperature range of 20 to 500 °C and the piezoelectric coefficients d_{33} were recorded using a quasi-static piezoelectric d_{33} meter (YE2730 – Sinoceramics).

The magnetization at room temperature and as a function of the magnetic field was measured on a vibrating sample magnetometer (Lakeshore 7300). Hysteresis cycles were taken between +13 and -13 kOe.

The magnetoelectric voltage coefficient (α_{ME}) was determined from the magnetic field induced voltage measured across the sample employing a lock-in amplifier (NF model LI5640) and using a bias magnetic field up to 15kOe overlapped by ac magnetic field of 2 Oe at 1 kHz.

Results and discussion

Before starting the sintering of the magnetoelectric compound, the calcination temperature of ferrite powders was determined. Figure 1 shows the XRD diagrams of the powders calcined at different temperatures between 675 and 1050 °C. Figure 1 shows the crystalline evolution with the temperature from the hematite phase (Fe_2O_3, JCPDS card 33-664) to the spinel crystalline structure corresponding to the $Ni_{0.5}Co_{0.5}Fe_2O_4$ phase (JCPDS card 04-002-0422). The extension

of the main peak attributed to hematite at 33.15° (see Figure 1.b) shows a clear diminution of this phase with the calcination temperature increasing. Moreover, from the figure, this phase disappears when powders were calcined at 1050 °C. Consequently, 1050°C was established as the calcination temperature for the obtention of the ferrite phase.

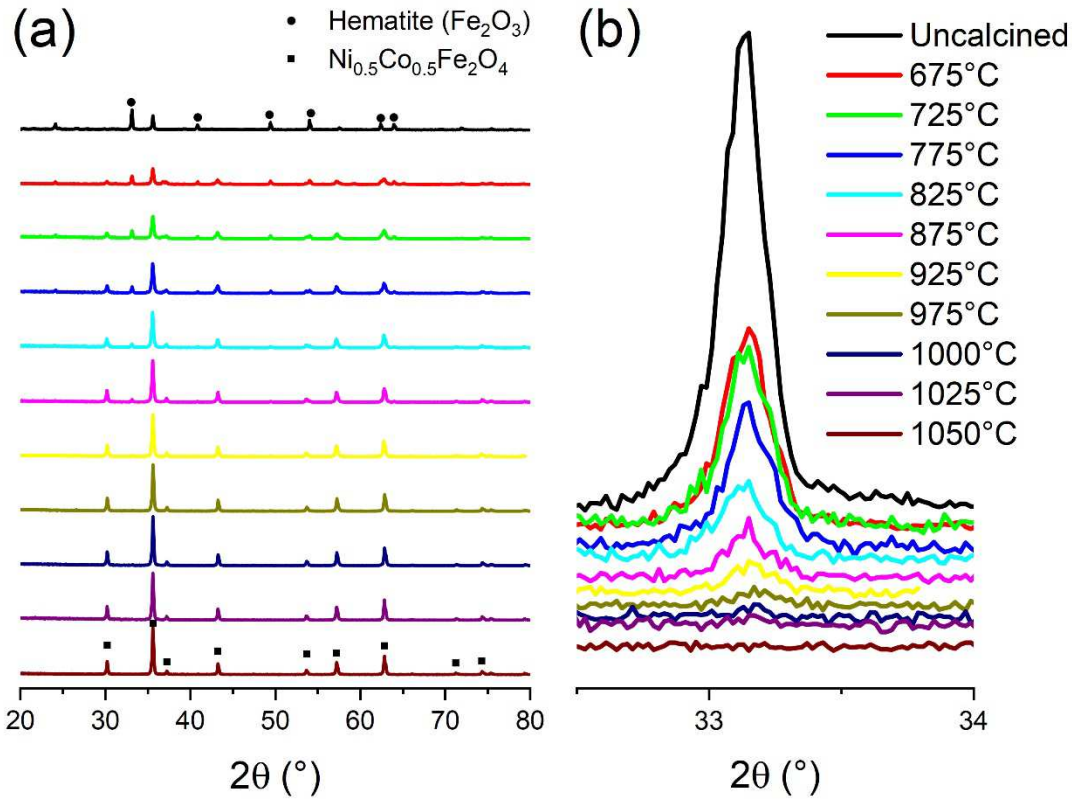

Figure 1. *(a) X-Ray Diffraction diagrams of NCF calcined powders between 675 and 1050 °C, (b) enlargement of the main peak of the Hematite phase at 33.2°.*

Figure 2 shows the XRD diagrams corresponding to sintered composites with different xBNKT-(100-x)NCF compositions. In the upper and lower part, diagrams of BNKT (perovskite) and NCF (spinel) are presented, respectively. In the main figure, a change in the peak intensities belonging to each phase can be observed. Analyzing the main peak of the NCF phase it is possible to observe a shift of it towards lower angles as the amount of BNKT phase increases indicating an expansion of lattice parameters due to the diffusion of larger radius ions into smaller ion-site in NCF material (Figure 3).

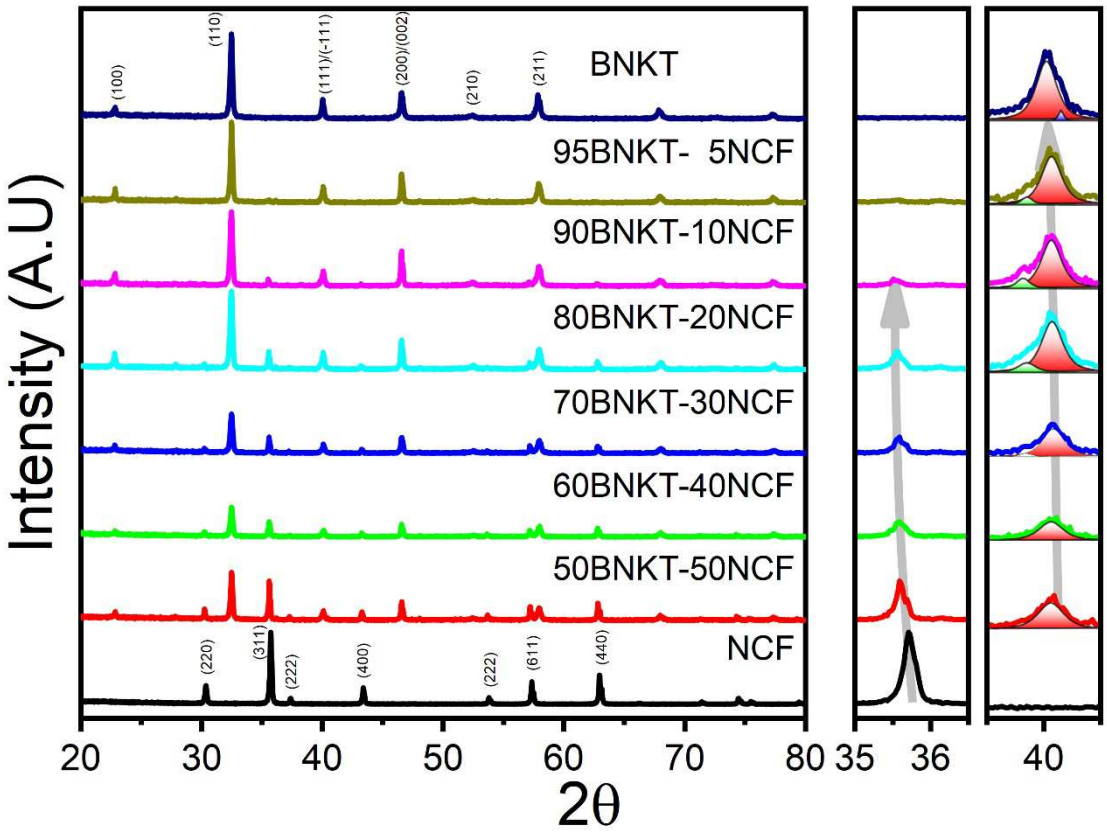

Figure 2. *XRD patterns of* $xBi_{0.5}(Na_{0.8}K_{0.2})_{0.5}TiO_3$-$(100\text{-}x)Ni_{0.5}Co_{0.5}Fe_2O_4$ *(x= 100, 95, 90, 80, 70, 60, 50, 0) composites sintered at 1100°C. Peaks corresponding to ferrite and piezoelectric phases were assigned according to bibliography.*[30,31]

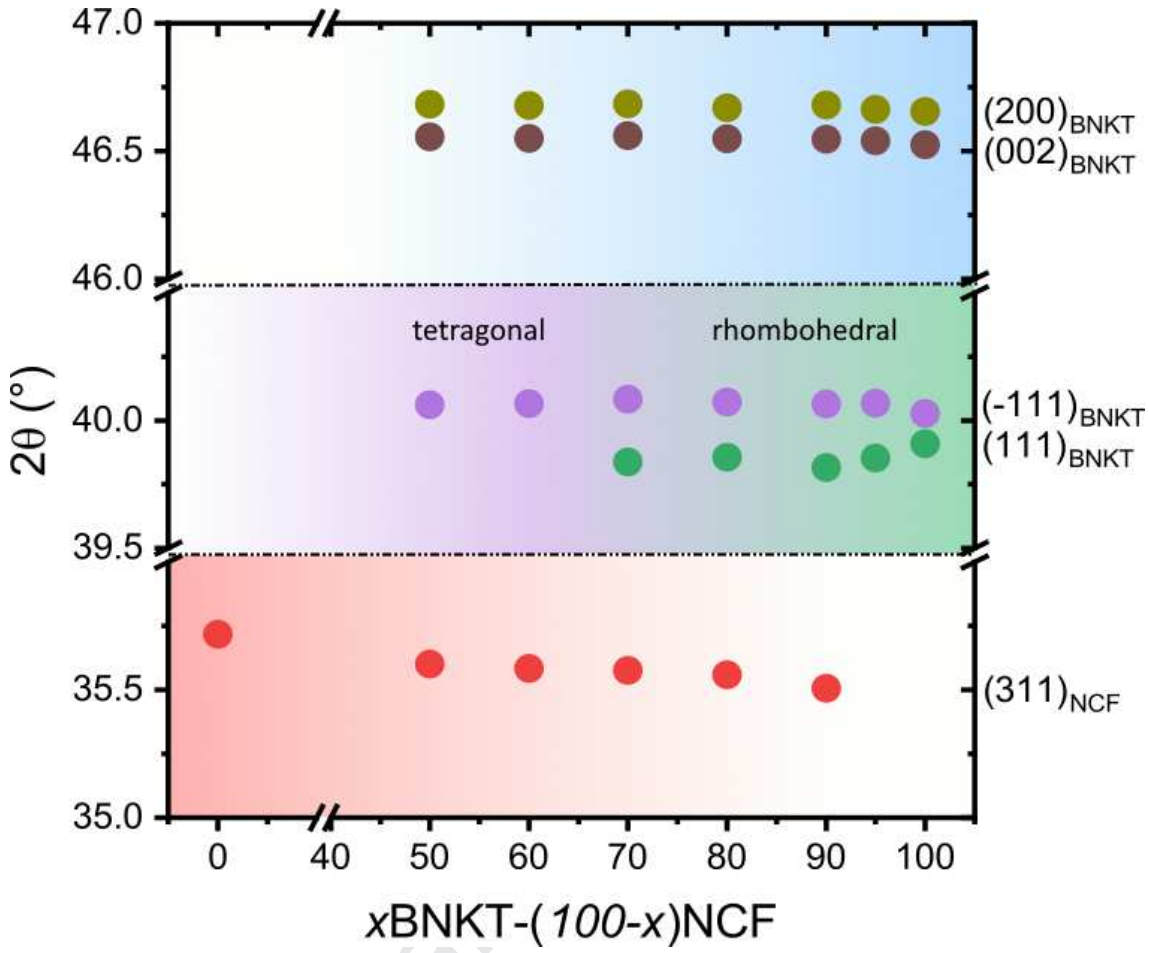

Figure 3. *Position peak evolution corresponding to (200)/(002) and (111)/(-111) planes of the BNKT phase and (311) plane of the NCF phase.*

In Figure 4, SEM images of sintered samples at 1100 °C for 5 hours are observed. From the figure, a significant increase in grain size as the content of NCF decreases is observed. Furthermore, the existence of a bimodal distribution of grain sizes and the formation of a secondary phase with bar-like morphology in 70/30 samples are detected.

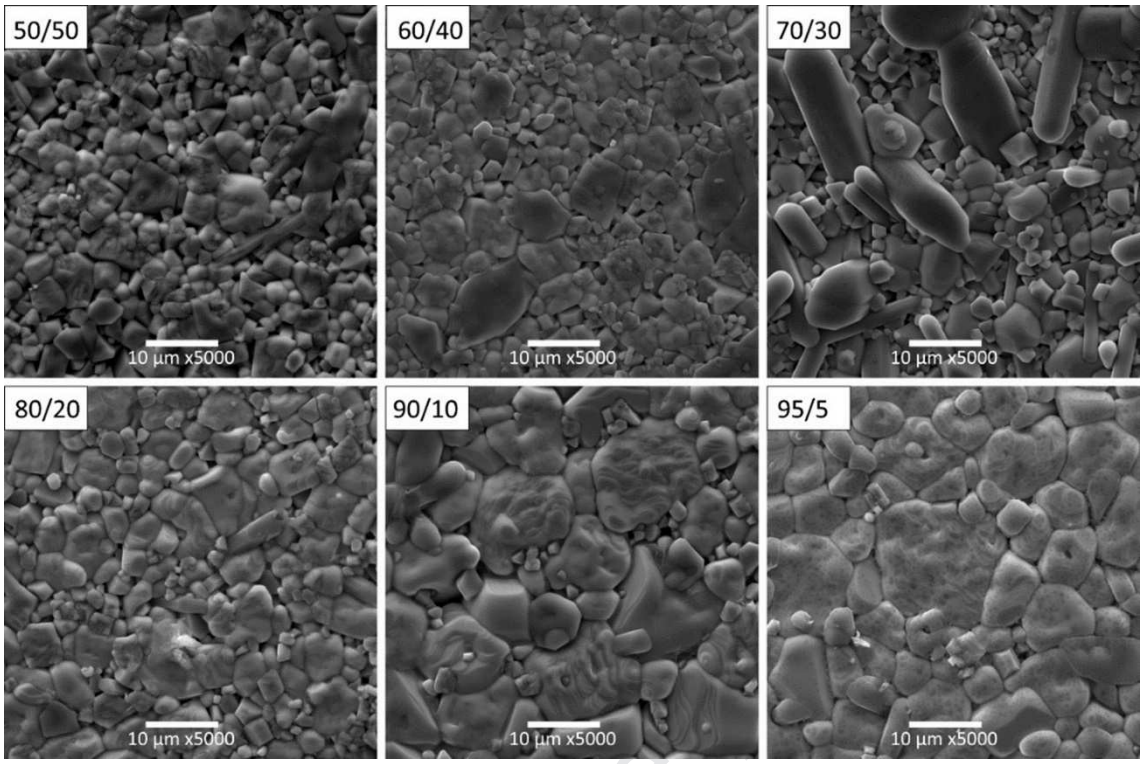

Figure 4. *SEM images of xBNKT-(100-x)NCF (x=95, 90, 80, 70, 60 and 50) sintered composites.*

Figure 5 displays the EDS mapping corresponding to the sample 90BNKT-10NCF. To analyze the distribution of different elements within the sample, the mapping corresponding to titanium is established as a reference in this work. From the analysis of elements distribution, it is possible to identify the presence of at least three phases. The first zone presents a high content of titanium and potassium ions, and a small amount of Fe, Ni and Co ions. Since in this area the bismuth content is below the detection limit of the technique, this zone is assigned to a secondary phase whose composition moves away from that corresponding to the ferrite and piezoelectric phases and shows similar composition to the previously reported in BNKT ceramics [32,33]. In the second zone, with less Ti intensity, a very similar stoichiometry to that of the BNKT system is observed. In this phase called “matrix”, a small amount of Fe, Co and Ni ions is detected. This observation is in agreement with the movement of the main peak of the BNKT phase observed by X-ray diffraction patterns. Analyzing the black zones in the titanium mapping, zones without titanium, the absence of bismuth and a high concentration of Fe, Ni and

Co are observed in the corresponding mappings. This third phase can be assigned to the NCF phase, where small amounts of K and Na are also found. These three zones are observed in all the samples analyzed by this technique. Moreover, it should be noted that for EDS analysis as the atoms mass decreases (like in potassium, sodium and especially oxygen) possible error raises. These results indicate that, although the ferrite and piezoelectric phases were synthesized separately, during the sintering process diffusion of different ions occurs, with the formation of a secondary phase and the corresponding change in the stoichiometric compositions of the piezoelectric and ferrite phases. Furthermore, this second phase and the increasing ferrite amount are responsible for the grain size diminution of the BNKT matrix.

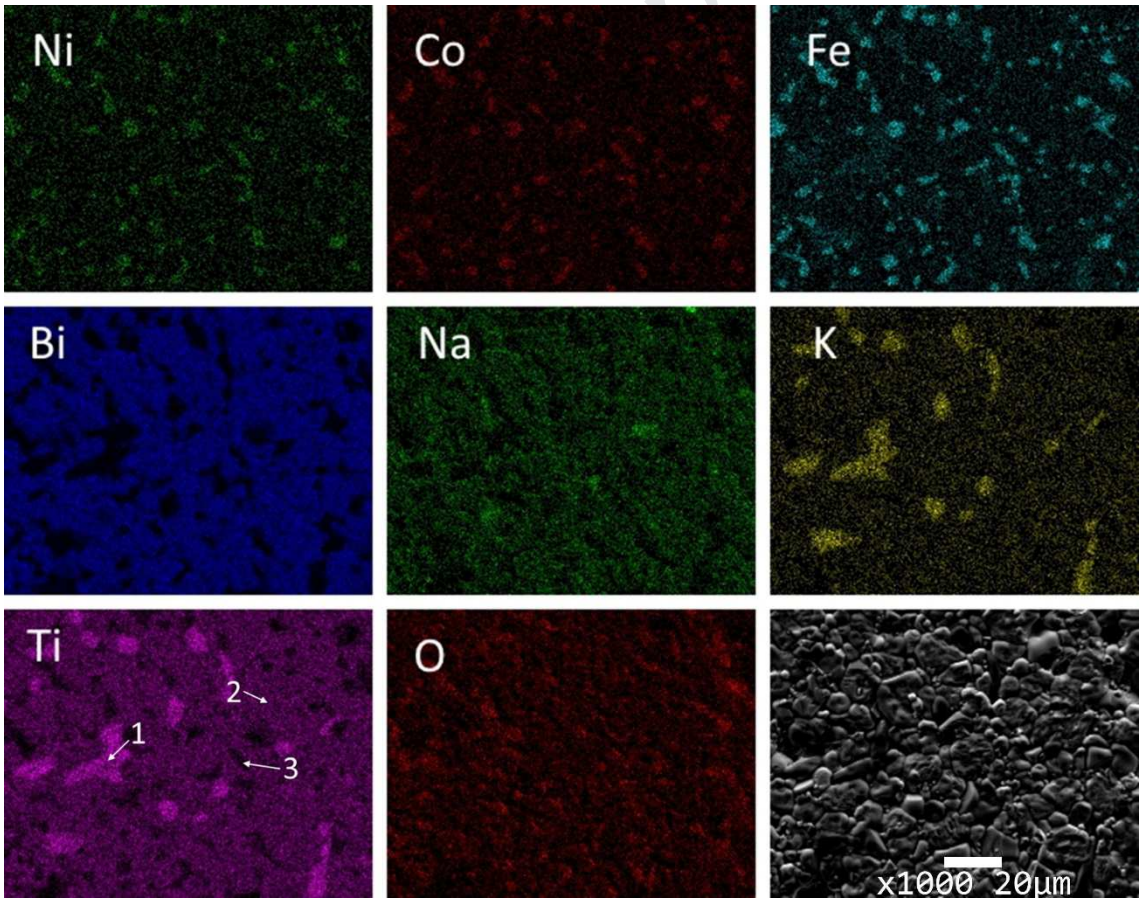

Figure 5. *EDS mapping of the different elements of 90BNKT–10NCF composite.*

Table 1 shows the experimental and calculated densities values of sintered samples. For calculation the Vegard's Law (Rule of Mixtures) was employed, taking into account the

theoretical densities of BNKT (5.97 g/cm³) [34] and NCF phases (5.334 g/cm³) [35]. The densification degree of composites was determined from calculated and measured densities values. From the table, it is possible to observe that all samples maintain a similar densification degree.

BNKT-NCF	Density (g/cm^3)	Calculated density (g/cm^3)	Densification degree (%)
50-50	5.17 ± 0.03	5.63	91.8
60-40	5.19 ± 0.02	5.70	91.1
70-30	5.32 ± 0.09	5.76	92.3
80-20	5.40 ± 0.08	5.83	92.6
90-10	5.45 ± 0.07	5.90	92.3
95-5	5.47 ± 0.06	5.93	92.2

Table 1. *Measured, and calculated density values and densification degree of sintered BNKT-NCF composites.*

Figure 6 shows the Raman spectra of *x*BNKT-(*100-x*)NCF sintered composites. For a better understanding, spectra of BNKT and NCF phases are also presented. For BNKT samples, four different characteristic bands are seen in the different regions of the spectrum. They are the 130 cm^{-1} mode related to A-site vibration in the perovskite structure, the around 240 and 400 cm^{-1} mode related to Ti-O vibration, the 430-700 cm^{-1} mode related to TiO_6 octahedra vibration, and above 700 cm^{-1} mode are related to A_1 and E longitudinal optical overlapping bands [36]. The splitting of bands between 200 and 400 cm^{-1} and the bands between 400 and 700 cm^{-1} are attributed to the presence of several ions at A-site (Bi^{+3}, Na^{+1}, K^{+1}). For pure NCF samples, five bands (corresponding to A_{1g}, E_g, and $3T_{2g}$ modes) in the Raman spectra that usually appear in the range of 150–750 cm^{-1} are identified. The A_{1g} mode corresponding to the symmetric stretch of oxygen atoms along (Fe/M)-O bond located at 700, 650 and 620 cm^{-1} can be assigned to Fe-O, Ni-O, and Co-O cations, respectively. The $T_{2g}(2)$ mode at 485 cm^{-1} corresponds to an anti-symmetric stretch of oxygen atoms along (Fe/M)-O bond. The E_g (327 cm^{-1}) and $T_{2g}(3)$ (570 cm^{-1}) are symmetric and antisymmetric bending modes of oxygen concerning Fe(M),

respectively. The $T_{2g}(1)$ mode situated at 213 cm^{-1} corresponds to the translational movement of tetrahedron MO_4 [37]. From the figure, a gradual band transition assigned to the pure BNKT phase to the ferrite bands as x increases is observed.

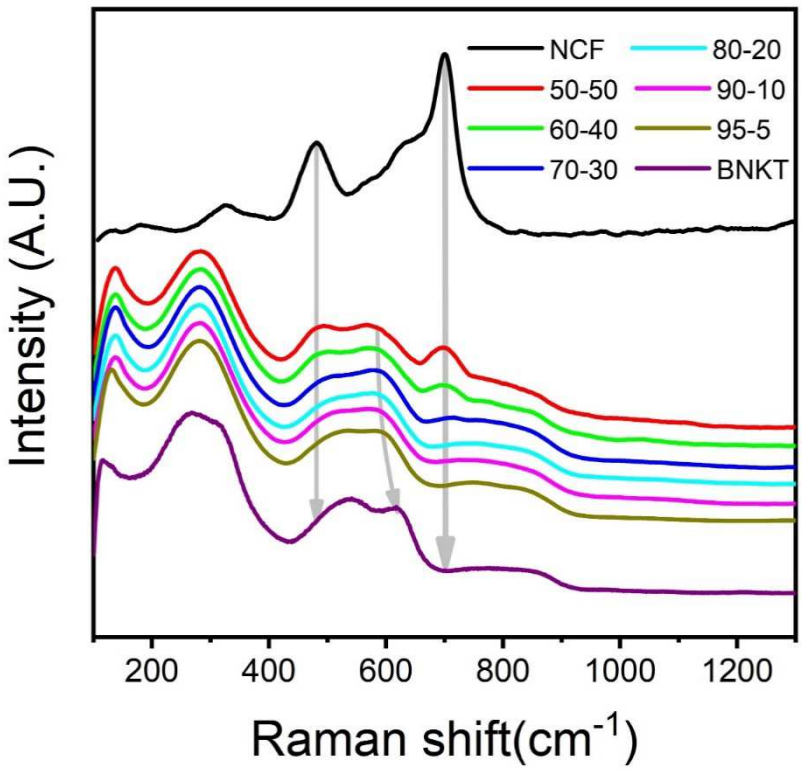

Figure 6. *Raman spectra of xBNKT-(100-x)NCF (x=100,95,90,80,70,60,50,0) composites.*

Figure 7 shows real permittivity and electrical loss curves as a function of the temperature of sintered composites. From the figure, real permittivity curves present two zones that are delimited by the maximum permittivity temperature of BNKT phase (~ 250 °C). The first zone, at temperatures below 250 °C, shows that the dielectric permittivity decreases and dielectric losses increase as the amount of NCF increases. In the second zone, temperatures greater than 250 °C, dielectric permittivity increases with the magnetic phase amount. This rise is associated with the greater ferrite conductivity with temperature. Furthermore, the 50BNKT-50NCF composite moves away from the permittivity values sequence indicating the percolation threshold. This result is also confirmed from elements mapping obtained through EDS (Figure

8), where an iron network is distinguished. This result indicates that the percolation limit of iron is stablished in the sample influencing dielectric properties.

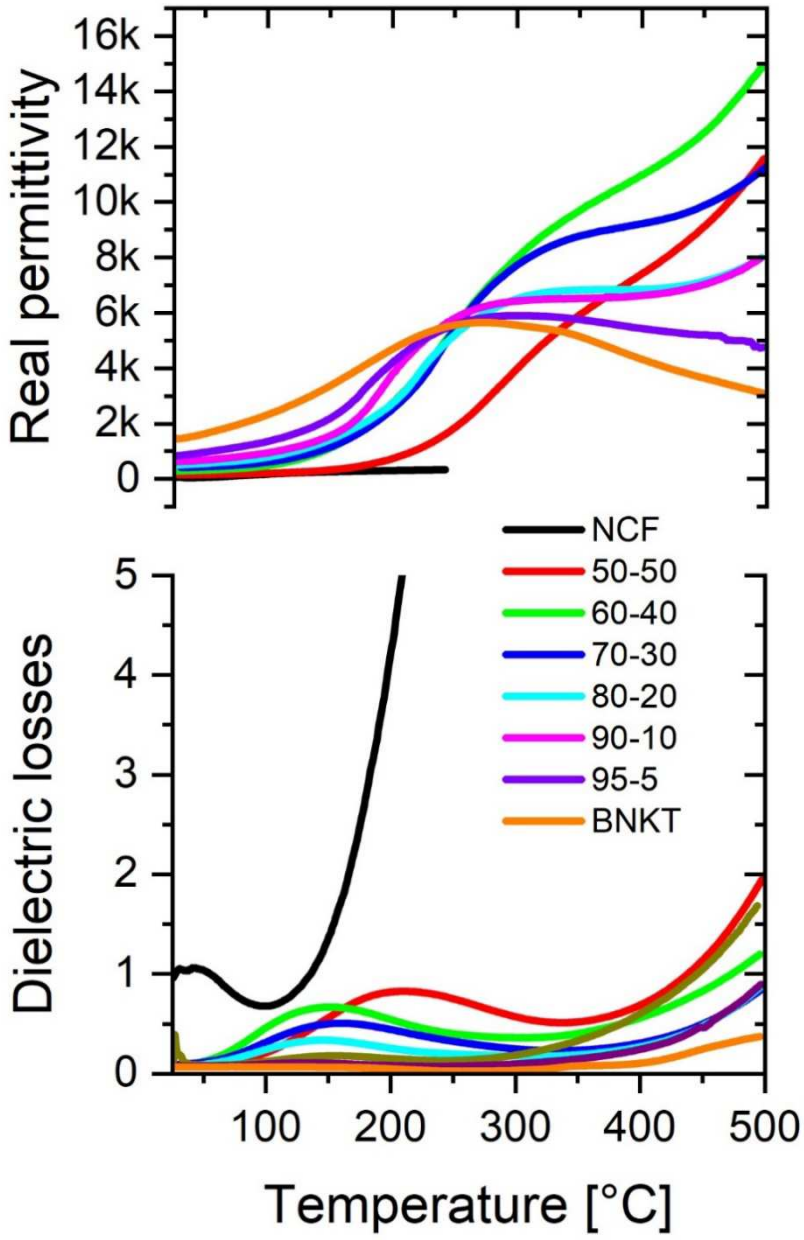

Figure 7. *Real permittivity and loss tangent vs. temperature of xBNKT-(100-x)NCF (x=100,95,90,80,70,60,50,0) composites.*

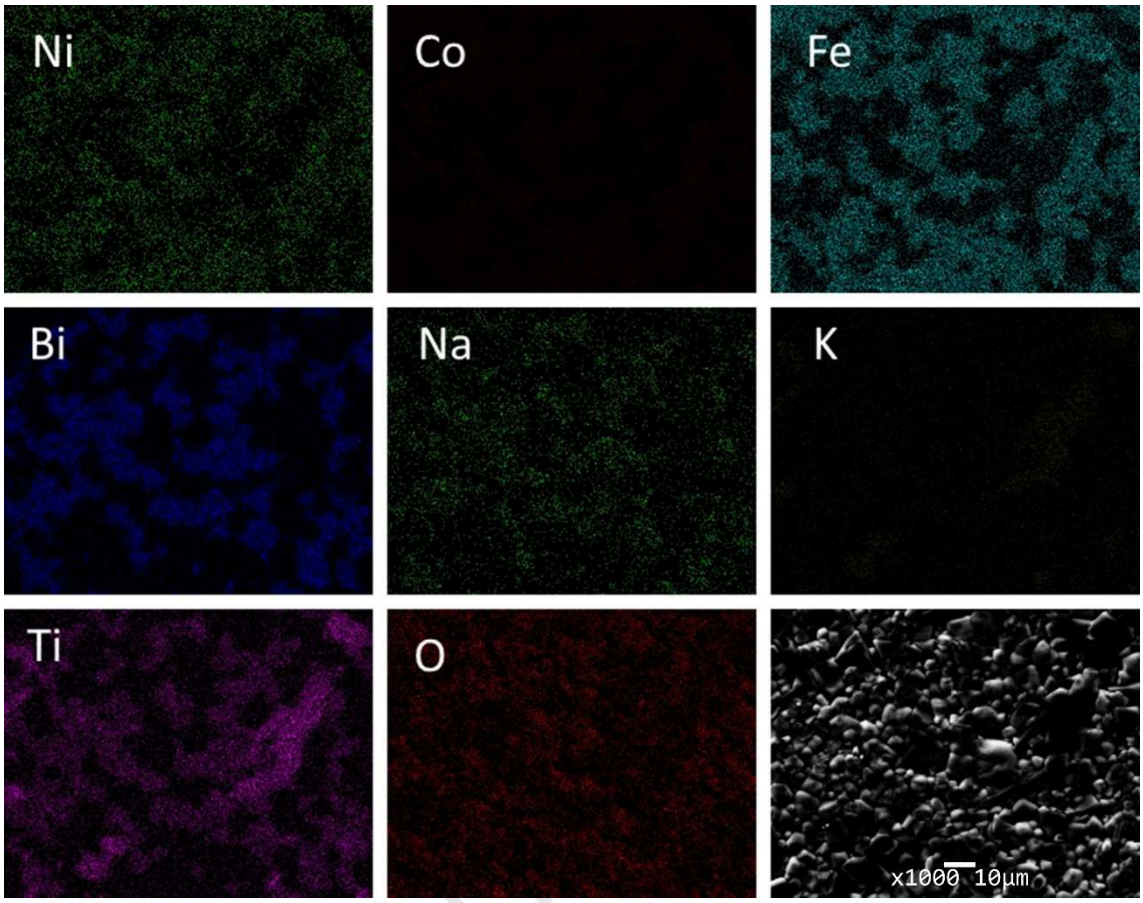

Figure 8. *Elements mapping corresponding to 50BNKT–50NCF composite.*

In Figure 9, the magnetic hysteresis behavior of pure ferrite samples is compared with the studied composites. Even though magnetization and coercive field are intrinsic properties of magnetic materials, they also depend on grain size and exchange interaction between magnetic grains. As can be seen in the figure and Table 2 and considering that NCF-phase is the only magnetic phase and magnetism fundamentally depends on the magnetic-phase content in the sample, a strong deviation from the linearity in the saturation magnetization (M_s) respect to the calculated from the Vegard's Law is registered. As it is evidenced by other techniques along with this work, part of the ions of the magnetic phase could migrate to the other phases (piezoelectric and secondary phases) and, therefore, BNKT-rich composites ($x \geq 80$) move away from linearity. Additionally, a decrease in the coercive magnetic field values when the piezoelectric phase increases could be related to the grain size growth which contributes to the domain wall movement.

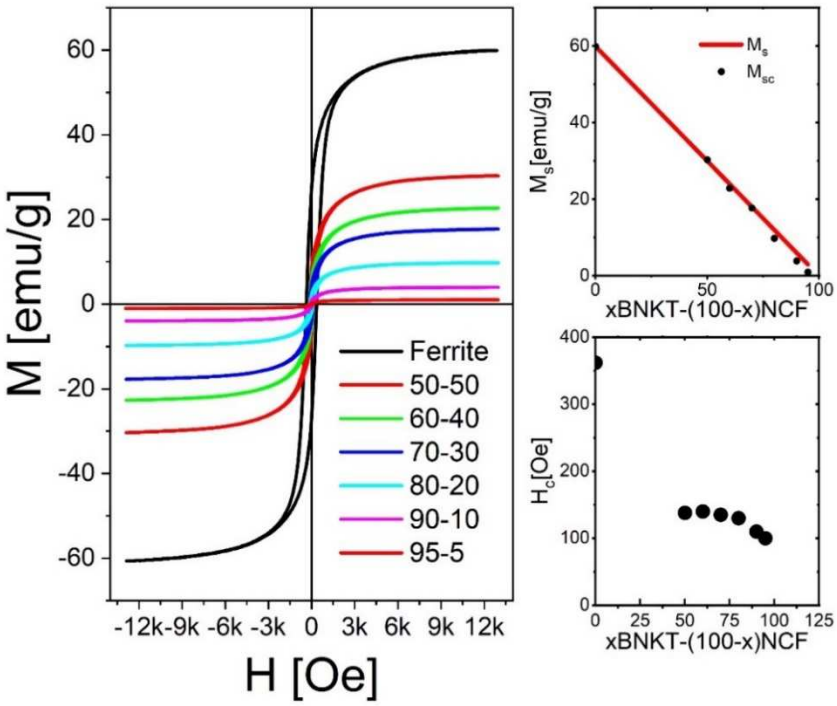

Figure 9. *Magnetic hysteresis loops of the pure NCF phase and xBNKT-(100-x)NCF composites (a), Saturation magnetization (b) and coercive magnetic field (c) evolution with composition.*

Sample	M_s (emu/g)	M_{sc} (emu/g)	H_c (Oe)
NCF	59.9	-	362
50/50	30.3	30.0	138
60/40	22.9	24.0	140
70/30	17.7	18.0	135
80/20	9.8	12.0	130
90/10	3.9	6.0	110
95/5	1.01	3.0	100

Table 2. Measured (M_s) and calculated (M_{sc}) saturation magnetization, and coercive field of sintered composites.

Figure 10 presents the magnetoelectric voltage coefficient as a function of the magnetic field for different NCF amounts. It is clear to see an increase of ME voltage with an increment of NCF amount reaching a maximum value when x=30 (70BNKT-30NCF composite). For higher NCF additions, the magnetoelectric voltage coefficient considerably decreases (see, 60BNKT-40NCF sample). In composites, the ME voltage coefficient is determined by the correlation

between piezoelectric, magnetostrictive, and microstructural parameters. Based on this fact, the increase in the ME coefficient with NCF amount until x=30 can be related to the enhancement of energy conversion due to the increase of magnetostrictive phase amount in spite of the decrease of d_{33} values (see Table 3). In addition, the porosity of composites is minimized for this NCF amount (as seen in Table 1). After x=30 it is possible to observe a degradation of d_{33} values and an increase in porosity suggesting an evanescence of mechanical coupling between phases and resulting in a decrease of ME voltage coefficient occurred by the percolation of magnetostrictive phase into the piezoelectric matrix, as suggested by dielectric properties of composites. It must be observed that at high fields, the typical sign-change of the magnetoelectric response of cobalt and nickel ferrites is detected. Effectively, due to the anisotropy of these ferrites, they compress until they overcome a certain magnetic field and then begin to dilate [38].

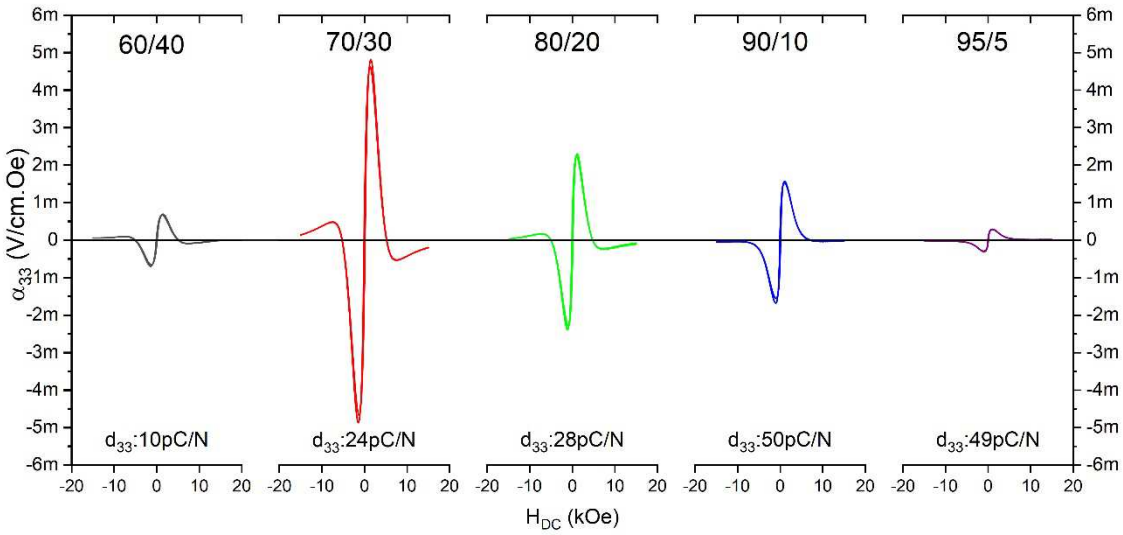

Figure 10. *Magnetoelectric voltage coefficient (α_{33}) vs. dc magnetic field of sintered composites using an ac magnetic field of 2Oe at 1kHz). Piezoelectric constant (d_{33}) of the composites is also reported in the figure.*

Sample	H_{DC} (kOe)	α_{33} (mV/cm.Oe)
60/40	1.444	0.695
70/30	1.452	4.816
80/20	1.150	2.241
90/10	1.021	1.567
95/05	0.915	0.287

Table 3. *DC magnetic field and magnetoelectric voltage coefficient (α_{33}) of sintered composites.*

Table 3 also shows the DC magnetic field values (H_{DC}) corresponding to the maximum magnetoelectric voltage coefficient of the xBNKT-(100-x)NCF composites. From the table, DC magnetic field increases with ferrite amount until the x=30, where the maximum magnetoelectric voltage coefficient is registered. Clearly, both values are influenced by the sample's composition, the mechanical coupling between phases and possible changes in the stoichiometry of ferrite and piezoelectric phases.

Conclusions

Magnetoelectric particulate composites were fabricated with $Bi_{0.5}(Na_{0.8}K_{0.2})_{0.5}TiO_3$ (BNKT) and $Ni_{0.5}Co_{0.5}Fe_2O_4$ (NCF) particles by the conventional ceramic processing. Taking into account the magnetoelectric voltage coefficient values in the of the BNKT-NCF composites, it can be concluded that the maximum value is obtained in a compromise between the piezoelectric constant (d_{33}) and the direct contact of both phases that can be influenced by the relative grain size of both phases. Indeed, for low ferrite phase addition, there is an excessive increase in the grain size of the piezoelectric phase which difficult the direct contact between the particles of both phases. On the contrary, the incorporation of a higher ferrite phase content inhibits the growth of the piezoelectric grains and favors the contact between both phases. These microstructural variations were accompanied by the existence of titanium and potassium-rich secondary phase and by the diffusion of iron, nickel and cobalt ions from ferrite to the BNKT phase, as well as the diffusion of potassium and sodium ions from piezoelectric to ferrite phase.

These compositional deviations and microstructural effects are responsible for moving away from the saturation magnetization and coercive magnetic field values from those calculated. Concluding, possible chemical reaction of the BNKT with ferrite and microstructural effects control magnetoelectric properties of lead-free composites.

Conflict of interest

The authors declare that they have no known competing financial interests or personal relationships that could have appeared to influence the work reported in this paper.

Acknowledgments

The authors would like to thank ANPCyT (PICT 2014-1314), CONICET and UNMdP for the financial support. The authors are also thankful to Dr. Paula Bercoff for the magnetic measurements.

References

[1] S.N. Babu, K. Srinivas, T. Bhimasankaram, Studies on lead-free multiferroic magnetoelectric composites, J. Magn. Magn. Mater. 321 (2009) 3764–3770. doi:10.1016/j.jmmm.2009.07.029.

[2] W. Eerenstein, N.D. Mathur, J.F. Scott, Multiferroic and magnetoelectric materials, Nature. 442 (2006) 759–765. doi:10.1038/nature05023.

[3] C.W. Nan, M.I. Bichurin, S. Dong, D. Viehland, G. Srinivasan, Multiferroic magnetoelectric composites: Historical perspective, status, and future directions, J. Appl. Phys. 103 (2008). doi:10.1063/1.2836410.

[4] C.M. Leung, J. Li, D. Viehland, X. Zhuang, A review on applications of magnetoelectric composites: From heterostructural uncooled magnetic sensors, energy harvesters to highly efficient power converters, J. Phys. D. Appl. Phys. 51 (2018). doi:10.1088/1361-6463/aac60b.

[5] N.X. Sun, G. Srinivasan, Voltage control of magnetism in multiferroic heterostructures and devices, SPIN. 02 (2012) 1240004. doi:10.1142/S2010324712400048.

[6] Y. Zhou, D. Maurya, Y. Yan, G. Srinivasan, E. Quandt, S. Priya, Self-Biased Magnetoelectric Composites: An Overview and Future Perspectives, Energy Harvest. Syst. 3 (2016) 1–42. doi:10.1515/ehs-2015-0003.

[7] M. Bichurin, V. Petrov, A. Zakharov, D. Kovalenko, S.C. Yang, D. Maurya, V. Bedekar, S. Priya, Magnetoelectric interactions in lead-based and lead-free composites, Materials (Basel). 4 (2010) 651–702. doi:10.3390/ma4040651.

[8] K.P. Jayachandran, J.M. Guedes, H.C. Rodrigues, Solutions for maximum coupling in multiferroic magnetoelectric composites by material design, Sci. Rep. 8 (2018). doi:10.1038/s41598-018-22964-9.

[9] Magnetoelectric Composites, Mater. Res. Soc. Symp. Proc. 1398 (2011). doi:10.1146/annurev-matsci-070909-104459.

[10] M. Etier, V. V. Shvartsman, S. Salamon, Y. Gao, H. Wende, D.C. Lupascu, The Direct and the Converse Magnetoelectric Effect in Multiferroic Cobalt Ferrite-Barium Titanate

Ceramic Composites, J. Am. Ceram. Soc. 99 (2016) 3623–3631. doi:10.1111/jace.14362.

[11] J. Wang, L. Song, K. Zhu, J. Qiu, Influence of Zr/Ti atomic ratio and seed layer on the magnetoelectric coupling of $Pb(Zr_xTi_{1-x})O_3$ film-on-$CoFe_2O_4$ bulk ceramic composites, Ceram. Int. 42 (2016) 14431–14437. doi:10.1016/J.CERAMINT.2016.06.039.

[12] S. Priya, R. Islam, S. Dong, D. Viehland, Recent advancements in magnetoelectric particulate and laminate composites, J. Electroceramics. 19 (2007) 149–166. doi:10.1007/s10832-007-9042-5.

[13] R. Grössinger, G. V. Duong, R. Sato-Turtelli, The physics of magnetoelectric composites, J. Magn. Magn. Mater. 320 (2008) 1972–1977. doi:10.1016/j.jmmm.2008.02.031.

[14] D. Maurya, M. Peddigari, M.G. Kang, L.D. Geng, N. Sharpes, V. Annapureddy, H. Palneedi, R. Sriramdas, Y. Yan, H.C. Song, Y.U. Wang, J. Ryu, S. Priya, Lead-free piezoelectric materials and composites for high power density energy harvesting, J. Mater. Res. 33 (2018) 2235–2263. doi:10.1557/jmr.2018.172.

[15] R.V. Krishnaiah, A. Srinivas, S.V. Kamat, T. Karthik, S. Asthana, Effect of $CoFe_2O_4$ mole percentage on multiferroic and magnetoelectric properties of $Na_{0.5}Bi_{0.5}TiO_3/CoFe_2O_4$ particulate composites, Ceram. Int. 40 (2014) 7799–7804. doi:10.1016/J.CERAMINT.2013.12.123.

[16] X.M. Chen, Y.H. Tang, I.-W. Chen, Z.C. Xu, S.Y. Wu, Dielectric and Magnetoelectric Characterization of $CoFe_2O_4/Sr_{0.5}Ba_{0.5}Nb_2O_6$ Composites, J. Appl. Phys. 96 (2004) 6520–6522. doi:10.1063/1.1809771.

[17] V. Röbisch, E. Yarar, N.O. Urs, I. Teliban, R. Knöchel, J. McCord, E. Quandt, D. Meyners, Exchange biased magnetoelectric composites for magnetic field sensor application by frequency conversion, J. Appl. Phys. 117 (2015) 17B513. doi:10.1063/1.4913814.

[18] G. Sreenivasulu, L.Y. Fetisov, Y.K. Fetisov, G. Srinivasan, Piezoelectric single crystal langatate and ferromagnetic composites: Studies on low-frequency and resonance

magnetoelectric effects, Appl. Phys. Lett. 100 (2012) 052901. doi:10.1063/1.3679661.

[19] H. Yang, J. Zhang, Y. Lin, T. Wang, High Curie temperature and enhanced magnetoelectric properties of the laminated Li0.058 (Na0.535 K0.48)0.942 NbO3/Co0.6 Zn0.4 Fe1.7 Mn0.3 O4 composites, Sci. Rep. 7 (2017). doi:10.1038/srep44855.

[20] A.S. Kumar, C.S.C. Lekha, S. Vivek, V. Saravanan, K. Nandakumar, S.S. Nair, Journal of Magnetism and Magnetic Materials Multiferroic and magnetoelectric properties, J. Magn. Magn. Mater. 33 (2016) 1–6. doi:10.1016/j.jmmm.2016.02.065.

[21] R.A. Islam, S. Priya, Magnetoelectric properties of the lead-free cofired BaTiO3 - (Ni0.8Zn0.2)Fe2O4 bilayer composite, Appl. Phys. Lett. 89 (2006). doi:10.1063/1.2361180.

[22] S.M. Mane, S.A. Pawar, D.S. Patil, S.B. Kulkarni, N.T. Tayade, J.C. Shin, Magnetoelectric, magnetodielectric effect and dielectric, magnetic properties of microwave-sintered lead-free x(Co0.9Ni0.1Fe2O4)-(1-x)[0.5(Ba0.7Ca0.3TiO3)-0.5(BaZr0.2Ti0.8O3)] particulate multiferroic composite, Ceram. Int. (2019). doi:10.1016/j.ceramint.2019.10.038.

[23] A. Prado-Espinosa, J. Camargo, L. Ramajo, M. Castro, Improvement on dielectric and microstructural properties of lead free Bi0.5Na0.5TiO3 ceramics through processing conditions, J. Mater. Sci. Mater. Electron. 28 (2017) 16836–16841. doi:10.1007/s10854-017-7599-6.

[24] T. Takenaka, K.I. Maruyama, K. Sakata, $(Bi_{1/2}Na_{1/2})TiO_3$ -$BaTiO_3$ System for Lead-Free Piezoelectric Ceramics, Jpn. J. Appl. Phys. 30 (1991) 2236–2239. doi:10.1143/JJAP.30.2236.

[25] A. Sasaki, T. Chiba, Y. Mamiya, E. Otsuki, Dielectric and Piezoelectric Properties of $(Bi_{0.5}Na_{0.5})TiO_3$–$(Bi_{0.5}K_{0.5})TiO_3$ Systems, Jpn. J. Appl. Phys. 38 (1999) 5564–5567. doi:10.1143/JJAP.38.5564.

[26] J. Camargo, L. Ramajo, F. Rubio-Marcos, M. Castro, Ferroelectric Properties of $Bi_{0.5}(Na_{0.8}K_{0.2})_{0.5}TiO_3$ Ceramics, Adv. Mater. Res. 975 (2014) 3–8. doi:10.4028/www.scientific.net/amr.975.3.

[27] A. Moosavi, M.A. Bahrevar, A.R. Aghaei, P. Ramos, M. Algueró, H. Amorín, High-field electromechanical response of $Bi_{0.5}Na_{0.5}TiO_3$–$Bi_{0.5}K_{0.5}TiO_3$ across its morphotropic phase boundary, J. Phys. D. Appl. Phys. 47 (2014) 055304. doi:10.1088/0022-3727/47/5/055304.

[28] J. Camargo, L. Ramajo, F. Rubio-Marcos, Y.M. Castro, Study of processing conditions of $(Bi_{0.5}(Na_{0.8}K_{0.2})_{0.5}TiO_3$, Bol. La Soc. Esp. Ceram. y Vidr. 53 (2014). doi:10.3989/cyv.42014.

[29] J. Camargo, A. Prado Espinosa, L. Ramajo, M. Castro, Influence of the sintering process on ferroelectric properties of $Bi_{0.5}(Na_{0.8}K_{0.2})_{0.5}TiO_3$ lead-free piezoelectric ceramics, J. Mater. Sci. Mater. Electron. (2018) 1–6. doi:10.1007/s10854-017-8508-8.

[30] P.P. Hankare, K.R. Sanadi, K.M. Garadkar, D.R. Patil, I.S. Mulla, Synthesis and characterization of nickel substituted cobalt ferrite nanoparticles by sol – gel auto-combustion method, J. Alloys Compd. 553 (2013) 383–388. doi:10.1016/j.jallcom.2012.11.181.

[31] G. Hernandez-Cuevas, J.R. Leyva Mendoza, P.E. García-Casillas, C.A. Rodríguez González, J.F. Hernandez-Paz, G. Herrera-Pérez, L. Fuentes-Cobas, S. Díaz de la Torre, O. Raymond-Herrera, H. Camacho-Montes, Effect of the sintering technique on the ferroelectric and d_{33} piezoelectric coefficients of $Bi_{0.5}(Na_{0.84}K_{0.16})_{0.5}TiO_3$ ceramic, J. Adv. Ceram. 8 (2019) 278–288. doi:10.1007/s40145-019-0314-8.

[32] L. Ramajo, J. Camargo, F. Rubio-Marcos, M. Castro, Influences of secondary phases on ferroelectric properties of $Bi(Na,K)TiO_3$ ceramics, Ceram. Int. 41 (2015) 5380–5386. doi:10.1016/j.ceramint.2014.12.100.

[33] A. Prado-espinosa, M. Castro, L. Ramajo, Influence of secondary phases on ferroelectric properties of $Bi_{0.5}Na_{0.5}TiO_3$ ceramics, Ceram. Int. 43 (2017) 5505–5508. doi:10.1016/j.ceramint.2017.01.071.

[34] J.-F. Trelcat, C. Courtois, M. Rguiti, A. Leriche, P.-H. Duvigneaud, T. Segato, Morphotropic phase boundary in the BNT–BT–BKT system, Ceram. Int. 38 (2012) 2823–2827. doi:10.1016/j.ceramint.2011.11.053.

[35] V.L. Mathe, R.B. Kamble, Anomalies in electrical and dielectric properties of nanocrystalline Ni–Co spinel ferrite, Mater. Res. Bull. 43 (2008) 2160–2165. doi:10.1016/J.MATERRESBULL.2007.09.001.

[36] D.K. Kushvaha, S.K. Rout, B. Tiwari, Structural, piezoelectric and highdensity energy storage properties of lead-free BNKT-BCZT solid solution, J. Alloys Compd. (2019) 270–276. doi:10.1016/j.jallcom.2018.12.196.

[37] B. Nandan, M.C. Bhatnagar, S.C. Kashyap, Cation distribution in nanocrystalline cobalt substituted nickel ferrites: X-ray diffraction and Raman spectroscopic investigations, J. Phys. Chem. Solids. 129 (2019) 298–306. doi:10.1016/j.jpcs.2019.01.017.

[38] R.M. Bozorth, E.F. Tilden, A.J. Williams, Anisotropy and magnetostriction of some ferrites, Phys. Rev. 99 (1955) 1788–1798. doi:10.1103/PhysRev.99.1788.

Highlights

The BNKT/NCF composites were synthesized via a activated solid state reaction method.

The influence of NCF on structural, functional properties was studied.

The composites exhibit ferrimagnetic as well as piezoelectric behavior.

Compositional deviations and microstructural effects influence magnetic parameters.

J. Camargo: Conceptualization, Investigation, Data Curation, Writing - Original Draft

A. Prado Espinosa: Investigation, Writing - Review & Editing

F. Zabotto: Resources, Writing - Review & Editing

L. Ramajo: Writing - Review & Editing, Supervision

M. Castro: Writing - Review & Editing, Supervision, Project administration

Declaration of interests

☒ The authors declare that they have no known competing financial interests or personal relationships that could have appeared to influence the work reported in this paper.

☐The authors declare the following financial interests/personal relationships which may be considered as potential competing interests: